Proteomics coupled with *AhR*-reporter gene bioassay for human and environmental safety assessment of sewage sludge and hydrochar

Claudia Landi [a,*], Giulia Liberatori [b], Monica Puccini [c], Enxhi Shaba [a], Lorenza Vantaggiato [a], Sandra Vitolo [c], Ilaria Corsi [b], Luca Bini [a]

[a] *Department of Life Sciences, University of Siena, Siena, Italy*
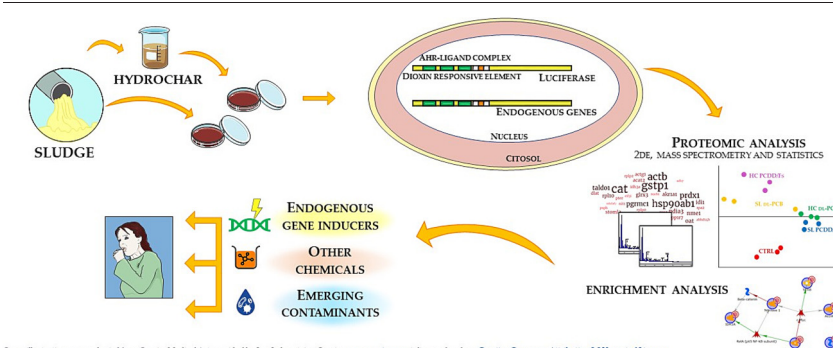[b] *Department of Physical, Earth and Environmental Sciences, University of Siena, Siena, Italy*
[c] *Department of Civil and Industrial Engineering, University of Pisa, Pisa, Italy*

HIGHLIGHTS

- DR-CALUX® exposed to SL and HC have been processed by proteomics.
- SL and HC treatments of DR-CALUX® cells determine peculiar protein profiles.
- Proteins act in antioxidant pathways, unfolded protein response and DNA damage.
- Proteomics suggests the enrichment of heavy metals in SL and HC.
- Proteomics showed a holistic scenario for the humans and environmental safety.

GRAPHICAL ABSTRACT

Some illustrations were adapted from Servier Medical Art provided by Les Laboratoires Servier www.servier.com is licensed under a Creative Commons Attribution 3.0 Unported License

ARTICLE INFO

ABSTRACT

Today application of sewage sludge (SL) and hydrochar (HC) in agriculture is a common practice for soil conditioning and crop fertilization, however safety concerns for human and environmental health due to the presence of toxic compounds have recently been expressed.

Our aim was to test the suitability of proteomics coupled with bioanalytical tools for unravelling mixture effects of these applications in human and environmental safety assessment. We conducted proteomic and bioinformatic analysis of cell cultures used in the DR-CALUX® bioassay to identify proteins differentially abundant after exposure to SL and the corresponding HC, rather than only using the Bioanalytical Toxicity Equivalents (BEQs) obtained by DR-CALUX®.

DR-CALUX® cells exposed to SL or HC showed a differential pattern of protein abundance depending on the type of SL and HC extract. The modified proteins are involved in antioxidant pathways, unfolded protein response and DNA damage that have close correlations with the effects of dioxin on biological systems and with onset of cancer and neurological disorders. Other cell response evidence suggested enrichment of heavy metals in the extracts.

The present combined approach represents an advance in the application of bioanalytical tools for safety assessment of complex mixtures such as SL and HC. It proved successful in screening proteins, the abundance of which is determined by SL and HC and by the biological activity of legacy toxic compounds, including organohalogens.

1. Introduction

Today application of sewage sludge (SL) in agriculture is a common practice for soil conditioning and crop fertilization, however safety concerns for human and environmental health due to the presence of toxic compounds have recently been expressed (Gianico et al., 2021; Gievers et al., 2019; Zhang et al., 2009). Sludge can deliver heavy metals, halogenated organic contaminants, drugs and personal care products, including biohazards such as pathogens (Clarke and Smith, 2011) with variable concentrations according to the type of wastewater (e.g. domestic vs. industrial) and treatment plant (e.g. aerobic vs. anaerobic) (Milieu Ltd et al., 2010). When SL is applied to soil, toxic compounds can be transferred to crops and terrestrial food webs, posing a hazard not only to humans but to entire terrestrial ecosystems (Protano et al., 2020; Tomczyk et al., 2021). Highly toxic compounds which may be delivered to topsoil include organohalogens, such as polyhalogenated dibenzo-*p*-dioxins (PCDDs), furans (PCDFs) and polychlorinated biphenyls (PCBs), which are absorbed by tiny carbonaceous soil particles (Hoogenboom et al., 2016; Yuan et al., 2021). Today soil pollution is a challenging issue, urgently requiring improved environmental risk assessment tools and management strategies. New technologies, such as thermal and hydrothermal treatment, have recently been proposed to recover and convert common low-value biomass such as SL (Huang and Tang, 2015). Hydrothermal carbonization, for instance, can convert SL into a carbonaceous solid at low temperatures (180–250 °C) and air pressures (10–40 bar) (Bardhan et al., 2021; Maniscalco et al., 2020; Tasca et al., 2020). The resulting hydrochar (HC) is an organic matrix containing a high percentage of carbon (>45–55 %), hydrogen and nutrients such as phosphorus (Azzaz et al., 2020; Masoumi et al., 2021). Application of HC as a soil amendment showed promising results in terms of improvement of soil quality and crop production, however the concerns about SL also apply to HC, since toxic chemicals in SL may persist after hydrothermal carbonization to HC (Rorat et al., 2019; Wiedner et al., 2013). This is all the more relevant due to the general consensus on placing regulatory limits on toxic chemicals in SL and HC in European countries (EU Sewage Sludge Directive, 86/278; Italian Legislative Decree 109/2018, *Genoa Decree*). Bioassays have been widely approved as screening tools for environmental and biological matrices and were recently recommended for wastewater and SL quality assessment (Barceló et al., 2020; Behnisch and Brouwer, 2020; Farré and Barceló, 2003; Kapanen et al., 2013; Macova et al., 2011; Neale et al., 2020; Selivanovskaya and Latypova, 2003). In particular, the Chemically Activated LUciferase eXpression (CALUX®) bioassay has been promoted for assessment of the occurrence and biological activity of organohalogenated compounds in certain complex environmental matrices, including SL (Addeck et al., 2014; Eljarrat and Barceló, 2004; Gustavsson et al., 2007, 2004; Houtman et al., 2020; Takigami et al., 2010; Van Langenhove et al., 2012; Zhang et al., 2009) and recently also biochar (Anderson et al., 2017; Lyu et al., 2016) and compost (Beníšek et al., 2015; Suzuki et al., 2004). Bioassays such as CALUX® could therefore be useful for assessing the safety of SL and HC for humans and the environment. In particular, the Dioxin Responsive (DR) CALUX® AhR reporter gene assay could be extremely useful for unravelling exposure to PCDD/Fs and dl-PCBs and the biological effects of SL and HC. We recently showed how this bioassay could be further implemented, since the rat hepatoma cells (H4IIE) used in this method are a biological system responsive to other chemicals and/or complex mixtures in sample extracts and activate molecular and biochemical responses by different cell pathways (Landi et al., 2021). Proteomics together with bioinformatics are promising tools for detecting modulation of proteins and molecular pathways indicating the effects that chemical mixtures may have on a given biological system. In turn, modulated proteins and molecular pathways may be considered targets of the chemical mixture, enabling us to infer environmental and human health risks. Current approaches to environmental risk assessment are challenging (Kumari and Kumar, 2020) and most are still limited to single-chemical toxicities (Heys et al., 2016). In order to model real situations it necessary to perform holistic studies that consider all the variables in a biological system. Analytical approaches cannot identify synergisms/antagonisms between physical and chemical stressors nor how a biological system responds. Effect-based tools are therefore far better descriptors of environmental exposure scenarios (Escher et al., 2020; Kortenkamp and Faust, 2018).

Here our aim was to use proteomics to study rat hepatoma cells (H4IIE) employed in the DR-CALUX® bioassay to screen for biological risks associated with exposure to SL and HC. Proteins detected by proteomic analysis which were differentially abundant after the different treatments were analysed by enrichment analysis in order to extract molecular pathways where the differential proteins act and determine diseases where these differential proteins are already known as biomarkers of protein modulation or contaminants that modulate proteins. These proteomic results were compared with our previous results based on bioanalytical toxicity equivalents (BEQs) obtained by DR-CALUX® (Liberatori et al., 2022).

In our first attempt to couple proteomics with H4IIE cells (DR-CALUX) using a topsoil sample from a highly industrialized area, we were able to extract several biological processes sensitive to particular drugs and compounds by bioinformatics and link them to the protein modifications identified (Landi et al., 2021). The altered biological pathways identified by proteomics reflected the complex epidemiological situation of persons living in the study area and underlined the need to investigate the sources of the drugs detected in the soil. The DR-CALUX bioassay coupled with proteomics revealed a more complex scenario of topsoil pollution and warrants further use and investigation as a tool in human and environmental risk assessment.

2. Methods

2.1. Chemicals

All DR-CALUX ® reagents were purchased from Gibco-Life Technologies (Carlsbad, CA, USA). Solvents used for extraction and purifications of SL and HC samples were pesticide residue grade and obtained from Sigma-Aldrich (St. Louis, MO, USA) and Biosolve Chimie (Dieuze, France). Dimethyl Sulfoxide (DMSO) was purchased from Sigma-Aldrich (St. Louis, MO, USA). Labelled standards for chemical analysis were purchased from Cambridge Isotope Laboratories (Andover, MA, USA) and Cerilliant (Round Rock, TX, USA). The 2,3,7,8-tetrachlorodibenzo-p-dioxin (TCDD) standard used for the bioassay calibration curve was acquired from Wellington Laboratories (Guelph, ON, Canada). Reagents for two-dimensional electrophoresis (2DE) and mass spectrometry analysis were obtained from Sigma-Aldrich (St. Louis, MO, USA), GE Healthcare (Uppsala, Sweden) and Bio-Rad Laboratories (Hercules, CA, USA).

2.2. SL and HC samples collection

Samples of SL were collected in 2019 from the wastewater treatment plant of the municipality of Florence (Italy). Aliquots of SL underwent hydrothermal carbonization under controlled laboratory conditions at the University of Pisa as previously reported (Tasca et al., 2020). The samples were transferred to the University of Siena in refrigerated containers at 4 °C, where they underwent DR- CALUX® bioassay and proteomics analysis. The study was performed in the framework of a large circular economy project funded by the Tuscan regional government (Sludge 4.0-POR FESR 2014–2020) on the treatment and transformation of biological sludge into biofertilizers.

2.3. SL and HC samples extraction for bioassay

SL and HC samples were extracted and purified prior to running the bioassay as previously described (Liberatori et al., 2022). Aliquots were processed as follows to obtain various extracts: SL aliquots (50 g) were lyophilized (Labogene, Scanvac cool safe) and HC aliquots (10 g) were oven dried (Memmert TM) at 105 °C for 1 h and then sieved (2 mm Ø). SL and HC samples were processed by Accelerated Solvent Extraction (ASE 200, Dionex™, Thermo Scientific) following a standardized protocol

reported in Behnisch et al. (2001, 2010) and Besselink et al. (2004) and briefly described as follows: 1–5 g of dried SL and HC samples were mixed with Dionex™ Prep Diatomaceous Earth (DE) and extracted with ASE in a mixture of hexane/acetone mixture (9/1); then a clean-up step was performed using a sulfuric acid silica column and then on Florisil cartridges (500 mg) to collect PCDD/Fs and dl-PCBs in separate fractions. The obtained fractions (PCDD/Fs and dl-PCBs) were dried under N flow and resuspended in DMSO.

The rat hepatoma cells (H4IIE) of the DR-CALUX bioassay were exposed to the following SL and HC extracts: two SL extracts containing the *dl*-PCB fraction and the PCDD/Fs fraction, respectively, and two HC extracts containing the *dl*-PCB fraction and the PCDD/Fs fraction, respectively. Controls consisting only of cells in their medium were included as previously reported (Landi et al., 2021). Three replicates (3 wells) of each SL and HC sample were run. After 24 h, the exposure media were transferred to a falcon tube; the cells were washed, trypsinized and resuspended in growth medium. The falcon tubes were centrifuged 3 times for 5 min at $1100 \times g$ at room temperature with 1 ml phosphate buffered saline (PBS) using the same protocol. The PBS was then discarded and the pellets stored at -80 °C until analysis. For proteomic analysis cell pellets were resuspended in 70 μl lysis buffer (7 M urea, 2 M thiourea, 4 % (*w/v*) 3-((3-cholamidopropyl) dimethylammonio)-1-propanesulfonate-CHAPS and 1 % (*w/v*) dithioerythritol-DTE) to extract total proteins. Protein concentration was then estimated by the Bradford assay (Kielkopf et al., 2020) before performing 2DE.

2.4. High resolution two-dimensional electrophoresis

Two-dimensional electrophoresis and image analysis were carried out as previously reported (Landi et al., 2021; Ontañon et al., 2018). Briefly, isoelectric focusing was performed with an Ettan™ IPGphor™ system on IPGstrips, an immobilized nonlinear gradient from pH 3 to 10, 18 cm in length, from Cytiva (Uppsala, Sweden, formerly GE Healthcare). The IPGstrips were rehydrated with 350 μl of sample containing 60 μg proteins for analytical runs and 600 μg for mass spectrometry (MS)-preparatory runs. Proteins were focused at 16 °C according to the following voltage program: 30 V for 6 h, 200 V for 2 h, a gradient to 3500 V in 2 h, a step at 3500 V for 2 h, from 3500 V to 5000 V in 2 h, maintained at 5000 V for another 3 h, a gradient to 8000 V in 1 h and a step at 8000 V for 3 h; finally, a gradient to 10,000 V in 1 h, maintained up to a total of 100,000 Vh. At the end of the isoelectric focusing (first dimensional run), the strips were washed with deionized water and equilibrated with two buffers, the first composed of 6 M urea, 2 % *w/v* Sodium Dodecyl Sulphate (SDS), 2 % w/v DTE, 30 % *v/v* glycerol and 0.05 M Tris–HCl pH 6.8 for 12 min and the second 6 M urea, 2 % w/v SDS, 2.5 % w/v iodoacetamide, 30 % v/v glycerol, 0.05 M Tris–HCl pH 6.8 and a trace of bromophenol blue for a further 5 min. Sodium dodecyl sulfate-polyacrylamide gel electrophoresis (SDS-PAGE) (second dimensional run) was performed on 9–16 % home-made polyacrylamide linear gradient gels at 40 mA/gel constant current at 9 °C. Analytical gels were stained with ammoniacal silver (Oakley et al., 1980), while MS-preparative gels were stained by a MS-compatible silver staining protocol (Landi et al., 2021; Sinha et al., 2001). Gel images were digitized by Image Scanner III coupled with LabScan 6.0 software (Cytiva, formerly GE Healthcare). Final gel images were compared by Melanie 9.0 software (Swiss Institute of Bioinformatics, Quartier Sorge, Batiment Amphipole 1015 Lausanne, Switzerland) to extract quantitative and qualitative differences. ANOVA statistical analysis was also performed with Melanie 9.0. Spots were considered differentially abundant when the ratio of mean relative percentage volumes (%V) was >1.5 with a statistical value of $p < 0.05$.

2.5. Mass spectrometry by MALDI ToF-ToF

Differentially abundant spots were excised from MS-compatible silver stained gel and analysed with a matrix-assisted laser desorption ionization time of flight (MALDI-ToF) Autoflex™ Speed mass spectrometer (Bruker Daltonics, Bremen, Germany) by a known protocol (Lanzafame et al.,

2021). Briefly, spots excised from the gel were decolorized in 30 mM potassium ferricyanide and 100 mM sodium thiosulfate mixed 1:1:2 with deionized water, then rinsed 6 times for 10 min each with water to stop the reaction. Next, 200 mM ammonium bicarbonate was added to cover the gel for 20 min and was then discarded. The spots were then washed with water and dehydrated with changes of 100 % acetonitrile (ACN) until the gel pieces turned opaque white. Spots were digested with 5 ± 10 ng/ml trypsin and 50 mM ammonium bicarbonate and incubated overnight at 37 °C. Tryptic peptides were eluted directly on the MALDI target and dried. Then 0.5 μl saturated α-cyano-4-hydroxycinnamic acid in 50 % ACN/0.1 % trifluoroacetic acid (TFA) solution was added to dried spots that were dried again. The MALDI target was inserted in the Autoflex™ Speed mass spectrometer and the spots were analysed. The MS spectra were processed by Flex Analysis software (Bruker Daltonics, Bremen, Germany).

Search parameters for protein identification by on-line Mascot search engine (Matrix Science Ltd., London, UK, http://www.matrixscience.com) were as follows: Swiss-Prot/TrEMBL databases; taxonomy limited to *Rattus* or *Mus musculus*; peptide mass fingerprint enzyme, trypsin; fixed modification, carbamidomethylation (Cys); variable modifications, oxidation of methionine; mass values, monoisotopic; ion charge state, $+1$; maximum miss cleavages, 1; mass tolerance, 50 ppm for peptide mass fingerprint and 0.6–0.8 Da for MS/MS. The mass spectrometry proteomics data is deposited with the ProteomeXchange Consortium via the PRIDE (Perez-Riverol et al., 2019) partner repository with the dataset identifier PXD040115.

2.6. PCA and Heatmap analysis

The relative volume percentage %V of differential spots was used to perform Principal Component Analysis (PCA) by XLStat version 2021.2.2 (Addinsoft, Paris, France, 2019), simplifying the amount of data by linear transformation. PCA made it possible to visualize experimental groups in two-dimensions on the basis of differential spot patterns.

To visualize the trend of spot abundance in all 2D-gels, heatmap analysis by a clustering method and Euclidean distance was performed on %V of statistically significant differentially abundant spots. The analysis and related figures were obtained by XLStat version 2021.2.2 (Addinsoft, 2019, Paris, France).

2.7. Enrichment analysis

2.7.1. MetaCore functional analysis

The protein spots were further processed by MetaCore™ version 22.1 build (Clarivate Analytics, Boston, MA, USA) including a manually annotated database of protein interactions, metabolic reactions and diseases obtained from the scientific literature. The UniProt accession numbers of the protein list (Table 1, AC column) were uploaded to MetaCore and processed. Enrichment analysis was based on the hypergeometric distribution algorithm and specific tools of MetaCore software such as protein network, canonical pathway modelling, pathway maps, process networks and disease biomarker networks. The results were then prioritized according to statistical significance.

2.7.2. Enrichr for drug dataset

Enrichr software is a comprehensive resource for curated gene sets, freely available at: https://maayanlab.cloud/Enrichr/ (Kuleshov et al., 2016). Enrichr is an easy to use intuitive enrichment analysis web-based tool providing various types of visualization summaries of collective functions of gene lists. The Enrichr search engine accumulates biological knowledge for biological discoveries on the basis of 427,081 curated terms, 203 libraries and 51,313,876 sets analysed (date: 12.10.2022), enabling powerful enrichment analysis. The gene names of the proteins identified (Table 1, "Gene Name" column) were uploaded to the Enrichr window. Pathways and "Disease/Drug" databases were considered for the analysis. In particular, we chose the Bioplanet 2019 database to discover molecular pathways involving the differential proteins and the Drug SIGnatures DataBase

Table 1

Statistical analysis results and MALDI ToF identifications. The table reports the proteins identified from the differential spots obtained by proteomic analysis, including spot number (i.e. that in the squares of Fig. 1A, Fig. 2 and Table S1), protein name, UniProt name and accession number (AC), gene name, theoretical isoelectric point (pI) and molecular weight (MW). Fold change is the ratio of the highest spot mean %V (#) to the lowest spot mean %V (§) between H4IIE cells treated with SL dl-PCBs, SL PCDD/Fs, HC dl-PCBs, HC PCDD/Fs and controls. Every spot reported satisfied one-factor ANOVA ($p < 0.05$). The table also reports the Mascot search results for protein identification parameters such as score, matched peptides and sequence cover percentage.

Spot n	Protein name	UniProt name (RAT)	AC	Gene name	pI MW	Fold	Anova (pvalue)	SL dl-PCB	SL PCDD/Fs	HC dl-PCB	HC PCDD/Fs	CTRL	Score	Matched Peptides	Coverage (%)
3	Sopentenyl-diphosphate Delta-isomerase 1	IDI1	O35760	Idi1	5.57–26,721	1.60	0.0006	1	0.014	0.013§	0.021#	0.02	96	7/12	29
18	Ornithine aminotransferase, mitochondrial	OAT	P04182	Oat	6.53–48,701	5.39	9×10^{-7}	0.06	0.07#	0.013§	0.017	0.053	171	15/37	48
21	2-iminobutanoate/2-iminopropanoate deaminase	RIDA	P52759	Rida	7.79–14,352	1.76	0.022	0.025	0.021	0.014§	0.021	0.03#	89	5/10	54
28	60S ribosomal protein L10	RL10	Q6PDV7	Rpl10	10.11–25,044	2.06	0.059	0.075§	0.155#	0.129	0.154	0.122	89	8/21	39
29	Peroxiredoxin-1	PRDX1	Q63716	Prdx1	8.27–22,327	1.63	0.024	0.161	0.172	0.155	0.238#	0.146§	242	15/21	62
31	Protein ABHD14B	ABHEB	Q6DGG1	Abhd14b	5.65–22,718	9.6	0.003	0.016	0.014	0.003§	0.026#	0.004	98	6/10	32
35	Glutathione S-transferase P	GSTP1	P04906	Gstp1	6.89–23,652	1.63	0.048	0.093#	0.082	0.057§	0.065	0.058	230	14/20	62
36	Phosphoserine phosphatase	SERB	Q5M819	Psph	5.49–25,180	2.04	0.041	0.023	0.018	0.017	0.033#	0.016§	187	12/17	64
37	Acetyl-CoA acetyltransferase, cytosolic	THIC	Q5XI22	Acat2	6.86–41,538	12.11	3×10^{-7}	0.199	0.238	0.275#	0.023§	0.247	196	6/13	24
40	All-trans-retinol dehydrogenase	ADH7	P41682	Adh7	6.60–40,878	5.90	11×10^{-4}	0.026	0.011§	0.013	0.062#	0.025	196	14/17	47
41	Phosphoserine phosphatase	SERB	Q5M819	Psph	5.49–25,180	5.08	11×10^{-4}	0.021	0.085#	0.067	0.017§	0.068	199	11/14	65
42	Inosine triphosphate pyrophosphatase	ITPA	D3ZW55	Itpa	5.48–22,261	1.54	3×10^{-4}	0.265§	0.311	0.384#	0.372	0.322	151	11/18	48
44	Membrane-associated progesterone receptor component 1	PGRC1	P70580	Pgrmc1	4.45–21,699	32.12	5×10^{-4}	0.042	0.018	0.003§	0.029	0.105#	140	8/12	40
46	Transaldolase	TALDO	Q9EQS0	Taldo1	6.57–37,610	2.64	13×10^{-4}	0.059#	0.050	0.022§	0.04	0.039	118	10/15	23
48	Phosphoserine phosphatase	SERB	Q5M819	Psph	5.49–25,180	17.69	0.0002	0.043	0.02	0.0052	0.093#	0.005§	237	14/22	70
51	Nucleoside diphosphate kinase A	NDKA	Q05982	Nme1	5.96–17,298	1.536	0.0007	0.078	0.108#	0.071§	0.097	0.079	152	11/23	70
53	Deaminated glutathione amidase	NIT1	Q7TQ94	Nit1	6.59–36,811	2.03	0.0011	0.036	0.028	0.023	0.045#	0.022§	165	12/18	42
54	Protein phosphatase 1 regulatory subunit 7	PP1R7	Q5HZV9	Ppp1r7	4.84–41,385	1.73	0.0011	0.177	0.109	0.106§	0.139	0.183#	294	19/24	65
55	Protein arginine methyltransferase NDUFAF7	NDUF7	Q5XI79	Ndufaf7	6.25–49,027	5.23	0.0013	0.063#	0.04	0.012§	0.058	0.046	77	6/11	19
56	Aldo-keto reductase family 1 member A1	AK1A1	P51635	Akr1a1	6.84–36,715	6.69	0.0016	0.051	0.029	0.013	0.084#	0.013§	251	20/37	51
59	60S acidic ribosomal protein P2	RLA2	P02401	Rplp2	4.44–11,685	34.06	0.0023	0.102	0.061	0.108§	0.085	0.003§	117	6/12	70
60	Isocitrate dehydrogenase [NAD] subunit alpha, mitochondrial	IDH3A	Q99NA5	Idh3a	6.47–40,044	2.11	0.0027	0.048	0.048	0.04	0.079#	0.038§	168	17/25	36 %
61	Glutaredoxin-3	GLRX3	Q9JLZ1	Glrx3	5.51–38,115	3.35	0.003	0.045	0.029	0.019§	0.062#	0.04	274	18/25	56
63	Elongation factor 2	EF2	P05197	Eef2	6.41–96,192	5.74	0.003	0.142#	0.077	0.082	0.096	0.025§	199	18/26	29
68	Stomatin-like protein 2, mitochondrial	STML2	Q4FZT0	Stoml2	8.74–38,504	2.20	0.004	0.117	0.097	0.072§	0.158#	0.081	153	9/13	42
71	Eukaryotic translation initiation factor 3	EIF3I	B0BNA7	Eif3i	5.38–36,837	1.95	0.012	0.165	0.186	0.122§	0.238#	0.172	258	17/22	52
72	60S acidic ribosomal protein P0	RLA0	P19945	Rplp0	5.91–34,365	3.98	0.013	0.021	0.022	0.056#	0.029	0.014§	108	8/16	37 %
73	Actin, cytoplasmic 1	ACTB	P60711	Actb	5.29–42,052	4.49	0.014	0.036	0.017§	0.076#	0.064	0.04	112	8/14	33
	Actin, cytoplasmic 2	ACTG	P63259	Actg1	5.31–42,108								112	8/15	33
75	Heat shock protein HSP 90-beta	HS90B	P34058	Hsp90ab1	4.97–83,571	2.41	0.016	0.026§	0.017	0.014	0.011§	0.015	167	14/15	20
77	Protein disulfide-isomerase A3	PDIA3	P11598	Pdia3	5.88–57,044	2.09	0.02	0.048§	0.074	0.067	0.100#	0.0812	177	15/21	32
79	Replication protein A 32 kDa subunit	RFA2	Q63528	Rpa2	5.47–29,499	2.02	0.020	0.047	0.04	0.032§	0.065#	0.036	121	8/17	47
80	Nucleobindin-1	NUCB1	Q63083	Nucb1	5.04–53,474	1.84	0.021	0.093#	0.064	0.078	0.05§	0.056	76	7/14	20
81	Dihydrolipoyllysine-residue acetyltransferase component of pyruvate dehydrogenase complex, mitochondrial	ODP2	P08461	Dlat	8.76–67,637	1.93	0.022	0.075§	0.039§	0.076#	0.072	0.05	215	15/18	32
82	Phosphotriesterase-related protein	PTER	Q63530	Pter	6.40–39,462	2.35	0.023	0.024	0.052	0.053	0.037§	0.057§	202	13/19	51
83	Catalase	CATA	P04762	Cat	7.07–60,062	2.44	0.035	0.014	0.008§	0.014	0.011	0.019#	148	12/20	27
85	40S ribosomal protein SA	RSSA	P38983	Rpsa	4.80–32,917	2.54	0.04	0.208	0.188	0.296#	0.249	0.117§	249	16/22	55

(DSigDB) to discover diseases/drugs related to the differential proteins that we found by proteomics. Statistical data (*p*-value, p-adjusted and related genes (proteins)) is reported.

2.8. Chemical analysis of SL and HC samples

Trace element analysis of the original SL and HC samples was carried out by EPA method 3052. An advanced microwave-digestion system was used. The extracts were analysed by ICP-MS iCAP Q System (ThermoFisher Scientific) as previously described (Liberatori et al., 2022).

The analytical determinations of PCDD, PCDFs and dl-PCBs in the SL and HC extracts tested on the rat hepatoma cells (H4IIE) (DR-CALUX bioassay) were carried out by EPA methods 1613B and 1668C using a Trace™ 1310 gas chromatograph (GC) equipped with DFS™ mass-spectrometer and a TriPlus™ RSH autosampler (all three from Thermo Scientific) according to the methods already described (Liberatori et al., 2022) for SL and HC samples. LOQ and LOD values were for total PAHs 0.005 mg/Kg d.w., total PCBs 5 µg/Kg d.w. and PCDD/Fs 0.15 ng/Kg d.w., respectively. Estimated concentrations of the PCDD/Fs and *dl*-PCB analytes detected were expressed in toxic equivalents (TEQ) and calculated by a known method (Van den Berg et al., 2006). Detailed information on extraction, clean-up and quantitation methods for SL and HC samples prior to gas chromatograph tandem mass spectrometry (GC–MS/MS) analysis of PCDD/Fs and *dl*-PCBs can be found in our previous study (Liberatori et al., 2022).

3. Results

3.1. Chemical analysis of SL and HC samples

As shown in Table 2, a general enrichment of inorganic and organic chemical compounds known for their biological reactivity and toxicity is observed in samples of SL and HC derived from SL. The only exception was Hg levels which showed an opposite trend, being higher in SL than HC. In particular, heavy metals as As, Cu, Pb and Zn almost doubled their values in HC compared to SL, similarly to Ni and Cr while Cd seems not to vary272.

3.2. Proteomic results of H4IIE cells treated with hydrochar and sewage sludge extracts

We compared the protein profiles of untreated H4IIE cells (control) and cells exposed to the four extracts (SL *dl*-PCBs, SL PCDD/Fs, HC *dl*-PCBs, HC PCDD/Fs) by proteomic analysis. The comparisons highlighted a total of 65 differential spots (Table S1; green numbers indicate higher mean %V; red numbers indicate lower mean %V). The greatest number of dysregulated spots was recorded for HC PCDD/Fs-treated cells (33/65) followed by HC *dl*-PCB- (8/65), SL PCDD/F- (6/65) and SL *dl*-PCB-treated cells (4/65).

Table 2
Contaminants in sewage sludge and hydrochar samples. Inorganic contaminants in mg/Kg dry weight; organic contaminants in toxic equivalents (TEQWHO) of 2,3,7,8 TCDD expressed as single dl-PCBs and PCDD/Fs and sum of dl-PCBs + PCDD/Fs, respectively.

Contaminants	Sludge	Hydrochar
Inorganic		
As	4.6	6.4
Cd	0.66	0.84
Cr	86	150
Hg	1.2	0.97
Ni	82	181
Pb	59	92
Cu	613	1090
Zn	523	890
Organic		
TEQWHO *dl*-PCBs	2.5	5.2
TEQWHO PCDD/Fs	3.3	12.9
TEQWHO PCDD/Fs + *dl*-PCBs	5.8	18.1

Ten spots showed different abundance between HC *dl*-PCB- and HC PCDD/Fs-treated cells (Fig. 1A, red and yellow intersecting circles in Venn diagram); likewise four spots differed between SL *dl*-PCB- and SL PCDD/Fs-treated cells (Fig. 1A, blue and green intersecting circles). Five spots distinguished SL *dl*-PCB- and HC *dl*-PCB-treated cells (Fig. 1A, blue and red intersecting circles) and four spots, SL PCDD/Fs- and HC PCDD/Fs-treated cells (Fig. 1A, green and yellow intersecting circles).

HC PCDD/Fs-treated cells also showed the greatest number of up-regulated proteins (22/66), followed by SL dl-PCB- (14/65), SL PCDD/F- (11/65) and HC dl-PCB-treated cells (10/65).

MALDI-ToF mass spectrometry analysis identified 39 proteins with the Mascot search engine (reported in Table 1 with score, matched peptides and % sequence cover). The differential proteins identified between controls and HC PCDD/F-treated cells were peroxiredoxin 1 (PRDX1), phosphoserine phosphatase (SERB), deaminated glutathione amidase (NIT1), aldo-keto reductase family 1 member A1 (AK1A1), isocitrate dehydrogenase [NAD] subunit alpha (IDH3A) and phosphotriesterase-related protein (PTER); those identified between controls and HC dl-PCB-treated cells were membrane-associated progesterone receptor component 1 (PGRC1), protein phosphatase 1 regulatory subunit 7 (PP1R7), 60S acidic ribosomal protein P2 (RLA2), 60S acidic ribosomal protein P0 (RLA0) and 40S ribosomal protein SA (RSSA). Differential proteins between HC *dl*-PCB- and HC PCDD/Fs-treated cells were eukaryotic translation initiation factor 3 (EIF3I), isopentenyl-diphosphate delta-isomerase 1 (IDI1), protein ABHD14B (ABHEB), replication protein A 32 kDa subunit (RFA2), acetyl-CoA acetyltransferase, cytosolic (THIC), phosphoserine phosphatase
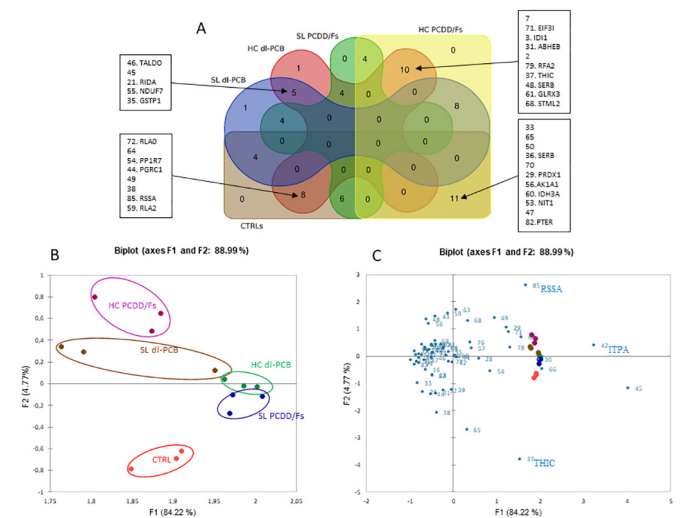
Fig. 1. Venn diagram and PCA. (A) Venn diagram showing the proteomic results. The red circle indicates the number of differential spots of HC dl-PCB-treated cells with respect to the other conditions, the green circle contains those of SL PCDD/Fs-treated cells, the yellow circle those of HC PCDD/Fs-treated cells, the blue circle those of SL dl-PCB-treated cells and the brown circle those of controls. The squares beside the Venn diagram contain (in clockwise order) the 10 differential spots with abbreviations of the protein names (when identified) between HC PCDD/Fs- and HC dl-PCB-treated cells, the 11 differential spots between HC PCDD/Fs-treated cells and controls, the 8 differential spots between HC dl-PCB-treated cells and controls and the 5 differential spots between SL dl-PCB- and HC dl-PCB-treated cells. (B) 2D representation of the principal components obtained by PCA for the 65 protein spots found to distinguish SL dl-PCBs-, SL PCDD/Fs-, HC dl-PCBs-, HC PCDD/Fs-treated cells and control samples. The histogram indicates dots representing our samples distributed on the basis of the differential spots detected by proteomic analysis. The colored circles indicate: magenta - HC PCDD/Fs samples, brown - SL dl-PCB samples, green - HC dl-PCB samples, blue - SL PCDD/Fs samples and red - controls. The first component F1 explains 84.22 % of the variance while the second component F2 explains 4.77 %. (C) The contributions of significant variants (differential spots) in the first two principal components, highlighting spots 85, 42, 45 and 37 as the most significant.

(SERB), glutaredoxin-3 (GLRX3) and stomatin-like protein 2, mitochondrial (STML2).

3.3. Multivariate analysis showed that HC PCDD/Fs-treated cell protein profile was the most distant from controls

Multivariate analysis was performed by Principal Component (PC) and heatmap analysis, uploading the %V of the 65 differentially abundant spots. PC analysis explained 88.99 % (F1: 84.22 % and F2: 4.77 %) of the variance (Fig. 1B). On the basis of the differential spot pattern obtained by proteomics, gel maps of H4IIE cells treated with the same extract clustered near each other and far from those of other treatments. In particular, maps of HC PCDD/Fs-treated cells (Fig. 1B; magenta dots) grouped far from those of controls (Fig. 1B; red dots). On the basis of the contributions of each significant variant in the first two PCs (Fig. 1C; light blue dots with numbers), spots 37, 42, 45 and 85 were the most significant for distinguishing the five groups of samples (Fig. 1C). Spot 37 represents acetyl-CoA acetyltransferase (THIC), down-regulated in HC PCDD/Fs-treated cells with respect to HC *dl*-PCB-treated cells. Spot 42 was identified as inosine triphosphate pyrophosphatase (ITPA), highly abundant in HC dl-PCB-treated cells and less abundant in SL dl-PCB-treated cells. Spot 85 was identified as 40S ribosomal protein SA (RSSA), up-regulated in HC dl-PCB-treated cells with respect to controls.

Heatmap analysis (Fig. 2) and PCA showed that samples with the same treatments clustered on the basis of differential spot pattern. That of H4IIE cells treated with HC PCDD/Fs (first three columns) was distinctive with respect to the other treatments. In particular, it showed an opposite trend of protein abundance with respect to control protein profiles (Fig. 2, cluster C_2 and C_6). Moreover, the trend of protein abundance in cluster C_6 was the opposite of that of HC PCDD/Fs- and HC dl-PCB-treated cells.

3.4. Enrichment analysis of all dysregulated proteins

In order to contextualize the differential proteins in terms of molecular interactions, process networks, pathway maps and disease biomarker networks, we performed MetaCore enrichment analysis. This functional ontology enrichment tool analyses uploaded data in gene ontology (GO) terms and provides a description of the biological functions, signalling mechanisms and pathologies in which the uploaded proteins are involved. Fig. 3 (legend in Fig. S1) shows the protein network built with all the dysregulated proteins found by proteomics based on the scientific literature. HS90B, GSTP1, CATA and NDPKA were central functional hubs (blue
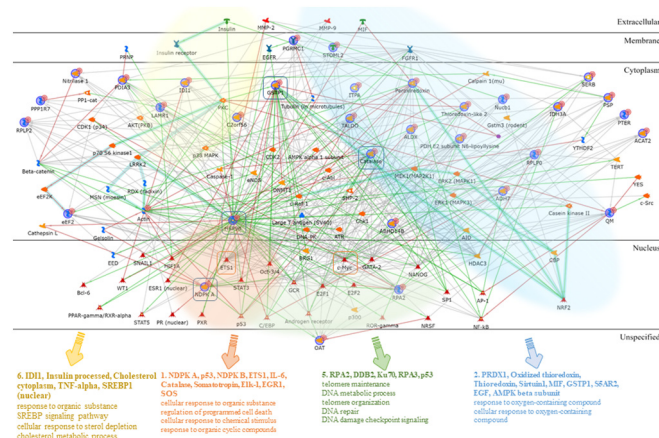

Fig. 3. MetaCore Protein network of all dysregulated proteins. Dysregulated proteins in H4IIE cells after treatment with SL dl-PCB, SL PCDD/Fs, HC dl-PCB and HC PCDD/Fs extracts were uploaded to MetaCore to obtain a theoretical protein network suggesting how these proteins interact with each other on the basis of the scientific literature. The protein network is distributed in cell localization mode: extracellular, membrane, cytoplasmic, nuclear and unspecified proteins. HS90B, GSTP1, CATA and NDKA are differential proteins considered to be central functional hubs (blue circles), i.e. proteins with many interactions with other proteins of the network. C-myc and ETS1 are transcriptional factors (orange circles) having the greatest number of links with the proteins identified. They could therefore have an impactful role in the protein modulation that we found by proteomic analysis. Bold turquoise lines represent canonical molecular paths, i.e. well-known molecular signal transduction cascades. Orange, blue, yellow and green clouds highlight the specific network areas of the canonical molecular paths of Table 3, reported together with gene ontology terms. The MetaCore legend can be found in Fig. S1.

circles), i.e. proteins with the greatest number of interactions and therefore important modulators of various molecular pathways down- and upstream. Numerous transcriptional factors are reported to be related to our proteins, in particular ETS1 and c-myc were linked to 28 of the proteins we identified. Canonical molecular pathways, indicated by bold turquoise lines and colored clouds and explained by the canonical pathway modelling results, are also associated with this protein network (Table 3; Fig. S2). Briefly, canonical path 1 (orange cloud in Fig. 3 protein network; Fig. S2) (NDPK A, p53, NDPK B, ETS1, IL-6) and path 4 (Fig. S2) (catalase, somatotropin, Elk-1, EGR1, SOS) are reported to be involved in cell response to organic substances, regulation of programmed cell death, cell response to chemical stimulus and response to organic cyclic compounds. Canonical path 2 (light blue cloud in Fig. 3; Fig. S2) (PRDX1, oxidized thioredoxin, thioredoxin, sirtuin1, MIF) and path 3 (Fig. S2) (GSTP1, sirtuin 1, S5AR2, EGF, AMPK beta subunit) are involved in response to oxygen-containing, organic cyclic and organonitrogen compounds. Canonical path 6 (yellow cloud in Fig. 3; Fig. S2) (IDI1, insulin processed, cholesterol cytoplasm, TNF-alpha, SREBP1) is related to response to cyclic organic compounds, oxygen-containing compounds, SREBP signalling pathway, cell response to sterol depletion and cholesterol metabolic process, while path 5 (green cloud in Fig. 3; Fig. S2) (RPA2, DDB2, Ku70, RPA3, p53) is related to telomere maintenance, DNA metabolic process, telomere organization, DNA repair and DNA damage checkpoint signalling.

The pathway maps tool contextualized differential proteins in specific biological pathways (Fig. 4A) such as: regulation of the nuclear factor-erythroid 2-related factor 2 (NRF2)-antioxidant pathway (PRDX1, TALDO, CATA, ITPA, NDPKA, HS90B), role of sirtuin1 and PPAR-γ co-activator-1 α (PGC1)-alpha in activation of antioxidant defence system (GSTP1, PRDX1, CATA), chaperone pathway regulation (HS90B), influence of low doses of arsenite on glucose-stimulated insulin secretion (PRDX1, CATA), regulation of HIF-1 (RSSA, HS90B) and ATR activation by DNA damage (RFA2, HS90B) (Fig. 4A).
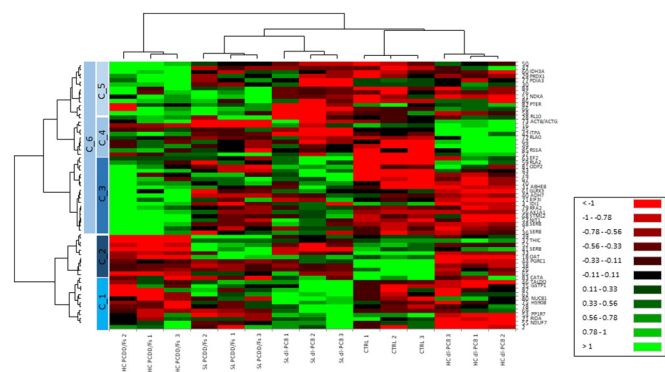

Fig. 2. Heatmap of proteomic results. Heatmap plotted with the 65 differential spots between SL dl-PCBs, SL PCDD/Fs, HC dl-PCBs, HC PCDD/Fs and control samples. The columns represent samples, named at the bottom. Rows represent differential spots, indicated on the right as numbers corresponding to those in Table 1 and the proteins identified are indicated by protein name abbreviations. Blue bars of different intensity on the left side of the heatmap represent the differential spot abundance clusters suggested by hierarchical clustering. The legend explains the heatmap colour scale from red (low abundance) to brilliant green (high abundance).

Table 3

Canonical pathway modelling. Canonical pathways were extracted by uploading the accession numbers of all dysregulated proteins to MetaCore (Canonical pathway modelling). The canonical pathways match well-known protein networks (Network) acting in specific biological processes (Gene ontology processes) reported with their statistical value (p < 0.05). Some of these protein networks are highlighted in the whole protein network of Fig. 3: i.e. 1) NDPK A, p53, NDPK B, ETS1, IL-6 (orange), 2) PRDX1, oxidized thioredoxin, thioredoxin, sirtuin1, MIF (light blue), 5) RPA2, DDB2, Ku70, RPA3, p53 (light green), 6) DI1, insulin processed, cholesterol cytoplasm, TNF-alpha, SREBP1 (nuclear) (yellow) and are reported individually in Fig. S2.

#	Network	GO processes	p-Value
1	NDPK A, p53, NDPK B, ETS1, IL-6	Response to organic substance (74.4 %; 5.351e-26), cellular response to organic substance (65.9 %; 4.369e-25), regulation of programmed cell death (54.9 %; 7.030e-25), response to oxygen-containing compound (59.8 %; 2.532e-24), regulation of apoptotic process (53.7 %; 3.694e-24)	9330E-116
2	PRDX1, Oxidized thioredoxin, Thioredoxin, Sirtuin1, MIF	Response to oxygen-containing compound (72.6 %; 1.351e-32), cellular response to oxygen-containing compound (60.3 %; 3.222e-29), response to organic cyclic compound (58.9 %; 7.396e-29), response to organic substance (78.1 %; 2.887e-26), response to organonitrogen compound (56.2 %; 5.912e-26)	1230E-94
3	GSTP1, Sirtuin1, S5AR2, EGF, AMPK beta subunit	Response to oxygen-containing compound (68.3 %; 7.174e-24), response to organic cyclic compound (56.7 %; 2.458e-22), cellular response to chemical stress (33.3 %; 8.614e-20), cellular response to oxygen-containing compound (53.3 %; 2.179e-19), metabolic process (96.7 %; 4.603e-19)	1090E-80
4	Catalase, Somatotropin, Elk-1, EGR1, ERK1/2	Response to organic cyclic compound (61.5 %; 5.542e-12), response to oxygen-containing compound (69.2 %; 2.328e-11), response to organic substance (80.8 %; 5.501e-11), response to organonitrogen compound (57.7 %; 1.441e-10), cellular response to oxygen-containing compound (57.7 %; 1.889e-10)	4740E-50
5	RPA2, DDB2, Ku70, RPA3, p53	Telomere maintenance (36.4 %; 2.033e-13), DNA metabolic process (59.1 %; 4.275e-13), telomere organization (36.4 %; 5.884e-13), DNA repair (50.0 %; 3.097e-12), DNA damage checkpoint signalling (36.4 %; 4.608e-12)	1050E-42
6	IDI1, Insulin processed, Cholesterol cytoplasm, TNF-alpha, SREBP1 (nuclear)	Response to organic cyclic compound (81.8 %; 5.699e-09), response to oxygen-containing compound (90.9 %; 7.664e-09), SREBP signalling pathway (27.3 %; 1.078e-08), cholesterol metabolic process (45.5 %; 1.129e-08), cellular response to sterol depletion (27.3 %; 1.436e-08)	2730E-24
7	LAMR1, COX-2 (PTGS2), Prostaglandin E2 extracellular region, HIF1A, Electron donor + Prostaglandin G2 = Electron acceptor + Prostaglandin H2 + H($_2$)O	Response to purine-containing compound (57.1 %; 1.260e-06), lactation (42.9 %; 1.263e-06), response to organic cyclic compound (85.7 %; 1.595e-06), negative regulation of intrinsic apoptotic signalling pathway in response to osmotic stress (28.6 %; 1.921e-06), cellular response to oxygen-containing compound (85.7 %; 2.125e-06)	2970E-14
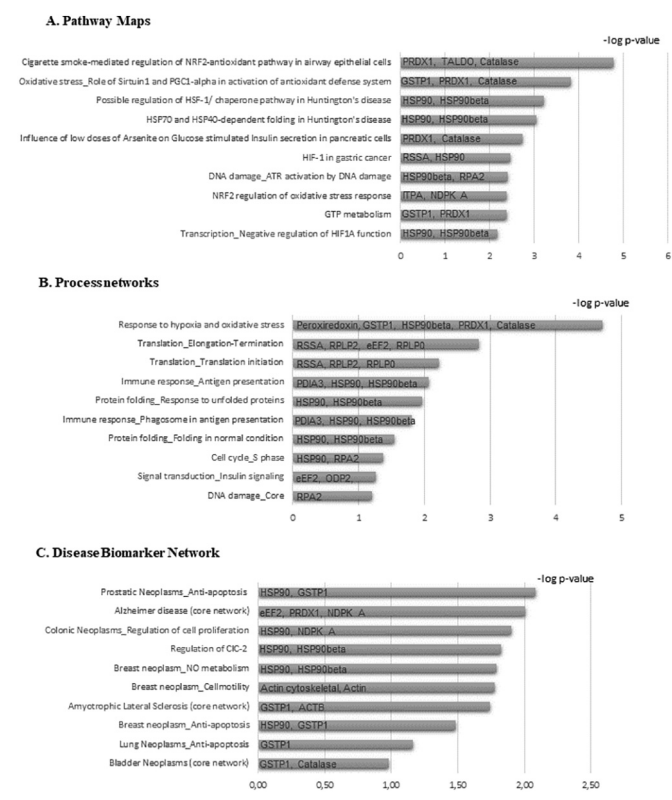
Fig. 4. MetaCore enrichment analysis of all dysregulated proteins. All differentially abundant proteins found comparing H4IIE cells after treatment with SL dl-PCB, SL PCDD/Fs, HC dl-PCB and HC PCDD/Fs extracts were uploaded to MetaCore for: (A) Pathway map analysis to obtain a statistically supported list of enriched molecular pathways where differential proteins are involved; (B) Process network analysis to obtain a statistically supported list of biological processes where differential proteins are involved and (C) Disease biomarker network construction to obtain a statistically supported list of diseases in which the proteins identified have been described as biomarkers. The histograms show the dysregulated proteins found by proteomic analysis.

The process networks tool signalled biological processes (Fig. 4B) such as response to hypoxia and oxidative stress (PRDX1, GSTP1, HS90B, CATA), translational processes (RSSA, RLA2, RLA0, EF2), response to unfolded proteins (HS90B), insulin signalling (EF2, ODP2) and DNA damage (HS90B, RFA2) (Fig. 4B).

The disease biomarker network tool highlighted diseases that may develop from altered modulation of the proteins identified. Fig. 4C reports pathologies such as prostate, colon, breast, lung and bladder cancer (HS90B, GSTP1, NDPKA, ACTB, CATA) and neurological disorders such as Alzheimer's disease and amyotrophic lateral sclerosis (EF2, PRDX1, NDPKA, GSTP1 and ACTB) where the differential proteins indicated have already been reported as biomarkers.
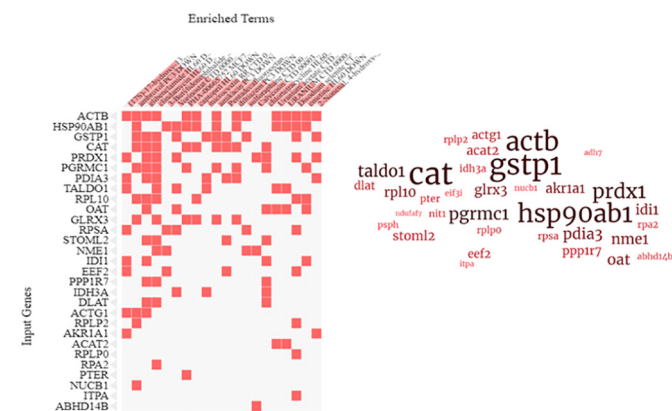
Fig. 5.

Enrichment analysis by Enrichr of all dysregulated proteins using DSigDB. Clustergram and word cloud of the Drug SIGnatures DataBase (DSigDB) results reported in Table S2. The clustergram highlights the most representative differential proteins interacting with drugs and compounds found in DSigDB. Columns show drugs and compounds that could interact with the abundant differential proteins shown in the rows. The word cloud highlights the most enriched differential proteins, suggesting the proteins which are modulated most by exposure to drugs and compounds.

Differential proteins were also analysed with the online Enrichr engine, taking Drug SIGnatures DataBase (DSigDB) results into consideration. This database reports drugs and compounds known to be correlated with the modulation of differential proteins found by proteomics. The complete results are reported in Table S2. The drugs and compounds linked to numerous differential proteins and with a valid *p*-value were ambroxol, glibenclamide, clindamycin, chlortetracycline, disodium selenite, copper sulfate, arsenenous acid, hydrogen peroxide, copper, lobeline, atrazine, cyclosporin, selenium, quercetin and benzo[*a*]pyrene. Fig. 5 shows a clustergram and a word cloud with the most frequent proteins that interact with the drugs and compounds of Table S2. ACTB, HS90B, GSTP1, CATA, PRDX1 and PGRC1 were proteins known to interact with many drugs and compounds of those in Table S2.

3.5. Enrichment analysis of differential proteins between controls and HC PCDD/Fs-treated H4IIE cells

Since we found a particularly abundant differential protein pattern between HC PCDD/Fs-treated cells and controls, we performed enrichment analysis to highlight the biological processes modulated by HC PCDD/Fs exposure. The protein network obtained by MetaCore (Fig. 6A) shows that AK1A1 (or ALDX), SERB, PRDX1, NIT1 and IDH3A have pivotal roles as central hubs. Transcriptional factors suggested to modulate and/or be modulated were c-myc and RelA (p65 NF-kB subunit). The biological processes (Fig. 6B) where these differential proteins were contextualized concern cell detoxification, cell response to toxic substances and removal of superoxide radicals.

Molecular pathways involved in these detoxification processes were obtained by Enrichr software from the BioPlanet 2019 database (Fig. 6C) and included benzo(*a*)pyrene metabolism (by AK1A1), amino acid biosynthesis and interconversion (transamination) (by PSPH or SERB), glycine, serine and threonine metabolism (by PSPH or SERB), pyruvate metabolism and the citric acid cycle (by IDH3A), glycerolipid metabolism (by AK1A1), the selenium pathway (PRDX1), androgen receptor proteolysis and transcription regulation (by PRDX1), and glycolysis and gluconeogenesis (by AK1A1) (Fig. 6C).

DSigDB results obtained by Enrichr (Table S3) show substances and drugs that may be correlated with modulations of the above molecular pathways. Aldo-keto reductase family 1 member A1 (AK1A1) modulation

Fig. 6. Enrichment analysis of proteins dysregulated in HC PCDD/Fs-treated H4IIE cells with respect to controls. Differential proteins found between HC PCDD/Fs-treated H4IIE cells and controls were uploaded to MetaCore to obtain: (A) a protein network suggesting how these proteins interact with each other on the basis of the scientific literature. AK1A1 (ALDX), SERB, PRDX1, NIT1 and IDH3A emerged as central hubs, i.e. proteins having a greater number of interactions with other proteins in the network; (B) Gene ontology biological processes where the differential proteins are involved. The differential proteins between HC PCDD/Fs-treated H4IIE cells and controls were also uploaded to Enrichr using molecular pathways in the BioPlanet 2019 database (C).

is reported to be related to exposure to copper, acrolein, 2-nonenal, 4-hydroxy-, (2E,4R), methylglyoxal, atrazine, nadide and benzo[*a*]pyrene-1,6-dione, benzo[*a*]pyrene-3,6-dione and benzo[*a*]pyrene-7,8-dione. Phosphoserine phosphatase SERB (PSPH) may be related to exposure to alexidine, quinpirole, atrazine, thapsigargin, dequalinium chloride and many other compounds. Indeed, IDH3A is related to exposure to copper, quinpirole, vorinostat, 2,6-dichloro-4-nitrophenol, oxidopamine and so forth. PRDX1 is related to exposure to copper, acrolein, 2-nonenal, 4-hydroxy-, (2E,4R), atrazine, vorinostat, cumene hydroperoxide, benzthiazide and other substances reported in Table S3.

4. Discussion

Human and environmental risk assessment of complex environmental matrices such as SL and HC is mandatory due to their increasing application in various sectors. Bioanalytical tools that couple exposure and the biological effects of complex matrices are useful for screening for toxic chemicals and their biological responses (Behnisch et al., 2001; Escher et al., 2020). Our recent efforts in coupling proteomics with DR-CALUX bioassay in soil samples from heavily contaminated industrial areas proved promising for human and environmental risk assessment (Landi et al., 2021). Other previous studies of ours showed several promising tools, such as the zebrafish embryotoxicity test coupled with behavioural traits, for assessing risks to aquatic wildlife from disposal of SL and HC in landfills (Della Torre et al., 2022).
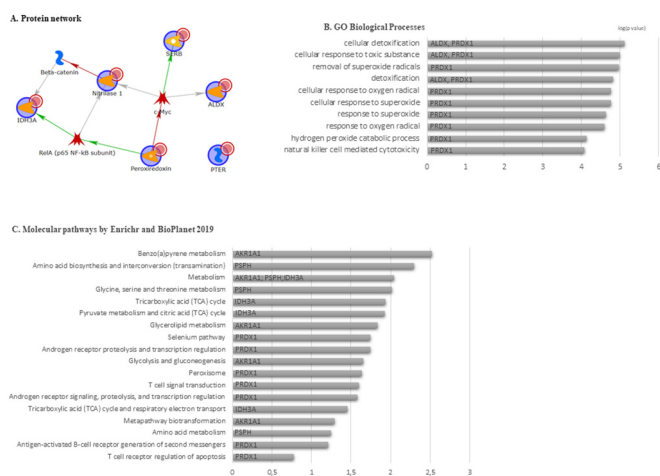
It was also demonstrated that DR-CALUX® is suitable for screening for legacy organohalogen compounds and biological activity in SL and HC matrices. This sustains use of the bioassay in the assessment of risks associated with environmental applications of SL and HC (Della Torre et al., 2022; Liberatori et al., 2022). The present study represents a further step in which DR-CALUX® H4IIE cells exposed to SL and HC extracts containing *dl*-PCBs and PCDD/Fs underwent proteomic analysis to identify proteins and molecular pathways targeted by compounds in SL and HC.

The DR-CALUX bioassay confirmed that SL and HC samples both contained *dl*-PCBs and PCDD/Fs with significantly higher BEQ values in HC samples ($p \leq 0.001$) (see data in Liberatori et al., 2022). In SL and HC, *dl*-PCB BEQ values were one order of magnitude higher than those of PCDD/Fs (SL 22.6 ± 6.5 vs 3.1 ± 0.4; HC 120.2 ± 31 vs 27.7 ± 4.7). A significant correlation was also found between BEQs and TEQs obtained by GC–MS analysis of SL and HC ($r > 0.8$) as reported in Liberatori et al. (2022).

Here we proposed combining proteomics with DR-CALUX H4IIE cells, which showed different protein profiles when treated with the four extracts (SL *dl*-PCB, SL PCDD/Fs, HC dl-PCB, HC PCDD/Fs). Principal component analysis showed that the groups of samples were not particularly well distinguished along PC1, whereas HC PCDD/Fs-treated cells and controls were the most distant samples along PC2. This suggests that stronger protein modulation was induced by exposure to HC PCDD/Fs. It is in line with the fact that the greatest number of dysregulated spots was found in HC PCDD/Fs-treated cells followed by HC *dl*-PCB-, SL PCDD/Fs- and SL *dl*-PCB-treated cells, in decreasing order.

The greatest contributions to PCA variability were due to spot 37, identified as THIC, spot 42 identified as ITPA, spot 45 and spot 85, identified as RSSA. All were up-regulated after HC *dl*-PCB treatment.

Functional analysis of the differential proteins in H4IIE cells after exposure to the four extracts showed that the biological processes most affected were antioxidant pathways, response to unfolded proteins and DNA repair mechanisms. Dysregulation of antioxidant pathways is suggested by different abundance of PRDX1, TALDO, CATA, GSTP1, ITPA and NDKA, in particular after exposure to SL and HC *dl*-PCB extracts. This mechanism was already reported in our previous study to be related to dioxin-mediated cytotoxicity via the aryl hydrocarbon receptor (*AhR*) (Della Torre et al., 2022). Interestingly, *AhR* is withheld in the cytoplasm by interaction with some chaperone proteins, including HS90B (Furue et al., 2021), that we found up-regulated after exposure to SL dl-PCBs and down-regulated after exposure to HC PCDD/Fs; our analysis indicated HS90B as a central functional hub in the protein network. On binding with dioxins, *AhR* leaves the chaperone complex and translocates into the nucleus, where it activates

transcription of xenobiotic response elements such as cytochrome P450 1A1(CYP1A1), CYP1A2 and CYP1B1. In particular, CYP1A1 metabolizes ligands and induces production of reactive oxygen species (Furue et al., 2021). The differential proteins tell us that the antioxidant pathways activated by H4IIE cells in response to the extracts were the Nrf2 and Sirt1/PGC1-alpha pathways.

The DNA repair mechanism (ATR pathway) found was another stress-activated signalling pathway normally responsive to exposure to extra- or intra-cellular stress which disrupts cell homeostasis and activates signalling pathways to rebalance intracellular biochemical processes (Hotamisligil and Davis, 2016; Maréchal and Zou, 2013; Rhind and Russell, 2012). In particular, Das and co-workers reported that oxidative stress produced by the *AhR* signalling pathway caused DNA damage in HaCaT cells and ITPA (Das et al., 2017) that we found up-regulated in HC *dl*-PCB-treated cells and that is one of the proteins dedicated to base excision repair mechanisms which may be impaired by oxidative stress. Interestingly, Panjali and co-workers reported that in peripheral blood of foundry workers, ITPA was strongly and positively correlated with concentrations of metal-rich airborne particulate (Panjali et al., 2021). This is in line with our previous study on the same batches of SL and HC, where heavy metals such as Cu, Hg and Zn were enriched in HC with respect to the SL source (Della Torre et al., 2022), a finding that sustains the hypothesis that hydrothermal carbonization may alter the content of selected toxic compounds. Data shown in Table 2 confirms a general enrichment of heavy metals in the conversion from SL to HC, that could explain the proteomic profile of ITPA.

Our disease biomarker network results suggest that some of the dysregulated proteins identified (HS90B, GSTP1, NDPKA, ACTB, CATA) are biomarkers of prostate, colon, breast, lung and bladder cancer. Indeed, Das and co-workers reported that an excessive number of DNA double-strand breaks produced by aberrant oxidative-stress-induced DNA recombination can lead to detrimental genetic changes and ultimately to carcinogenesis (Das et al., 2017). In addition to different kinds of cancer, our analysis suggests correlations with neurological disorders, such as Alzheimer's disease and amyotrophic lateral sclerosis, and dysregulation of proteins of neurological importance (EF2, PRDX1, NDPK, GSTP1, ACTB) in complex biological systems. We already demonstrated that zebrafish larvae exposed to SL and HC suffer significant impairment of swimming performance, probably due to chemicals such as heavy metals that affect behavioural traits (Della Torre et al., 2022). Their presence, confirmed by chemical analysis of SL and HC, and their effects, are also sustained by our DSigDB results that associate our differential proteins with Cu, As, benzo[*a*]pyrene-1,6-dione, benzo[*a*]pyrene-3,6-dione and benzo[*a*]pyrene-7,8-dione.

Since we detected a differential protein profile between HC PCDD/Fs-treated cells and controls, we performed a specific enrichment analysis. Proteins modulated after exposure to HC PCDD/Fs are involved in cell detoxification processes and removal of superoxide radicals. In this case, aldo-keto reductase family 1 member A1 (AK1A1 or ALDX) and PRDX1, both overexpressed in cells treated with HC PCDD/Fs, have central functional roles. Fuse and coworkers reported that these detoxifying enzymes and antioxidant proteins are induced by the transcription factor Nrf2 (as we found in complete analysis), conferring protection against the toxic effects of a range of chemicals (Fuse et al., 2016). In particular, modulation of PRDX1 could have different effects on the basis of its extracellular or intracellular localization: extracellular PRDX1 plays a pivotal role in regulating inflammation (Landi et al., 2014), while intracellular PRDX1 acts as a molecular chaperone that can modulate many molecules (Jang et al., 2004) and regulate transcriptional processes (Wang et al., 2010). PRDX1 expression is correlated with removal of superoxide radicals and with malignant disease (Landi et al., 2014; Rosenfeldt and Ryan, 2009).

AKR1A1 is an oxidoreductase (Iino et al., 2021). In line with our results, Balu and co-workers reported that it mediates genotoxicity in the presence of benzo[*a*]pyrene (Balu et al., 2004). As suggested by the protein networks (all differential proteins and differential proteins in controls vs HC PCDD/Fs), c-Myc has a central role especially in the complete protein network where it modulates 28 of the proteins we identified as well as transcriptional factor EST1. C-myc is a proto-oncogene involved in tumorigenesis

(Schaub et al., 2018) while EST1 is a regulatory subunit of telomerase required for telomerase activity in vivo: deletion of this subunit causes telomere shortening and cell senescence (Tong et al., 2011).

Interestingly, PRDX1 interacts with the transcriptional regulatory domain of the c-Myc oncoprotein and suppresses its transforming activity (Graves et al., 2009). AK1A1 (ALDX) is also related to c-Myc, which is reported to be its genomic target in humans (Fernandez et al., 2003). PRDX1 is also related to NF-kB in the network, and is known to differentially regulate NF-kB activity on the basis of its nuclear or cytoplasmic localization (Hansen et al., 2007). NF-kB is also related to nitrilase 1 (NIT1), that we found to be up-regulated in cells treated with HC PCDD/Fs. This protein is reported to suppress chemically induced carcinogenesis (Wang et al., 2016) and is considered a 'green' catalyst by virtue of its capacity to eliminate highly toxic nitriles. This and other nitrile-converting enzymes play an important role in environmental protection (Singh et al., 2006). Our data suggests that NIT1 could be modulated prevalently by Cu and arsenous acid, both confirmed to be present in SL and HC, as well as by thiostrepton, atrazine and thapsigargin.

In our network of proteins dysregulated by HC PCDD/Fs, IDH3A is also linked to RelA, the p65 NF-kB subunit. IDH3A is a rate-limiting enzyme of the citric acid cycle that irreversibly catalyses conversion of isocitrate to α-ketoglutarate in a reaction that depends on nicotinamide adenine dinucleotide (NAD+). Up-regulation of this enzyme has been correlated with protumorigenic effects through promotion of the epithelial-mesenchymal transition, thereby facilitating cancer cell migration and invasion (Liu and Sabatini, 2020; Liu et al., 2020). Phosphoserine phosphatase (SERB) is part of the serine synthesis pathway and recent studies cast new light on the role of serine metabolism in cancer, suggesting that active serine synthesis might be required to change metabolic fluxes after a cell's transformation to a malignant state or after the expression of specific oncogenes, as well as in response to alterations in nutrient availability and tissue environment (Cairns et al., 2011; Mattaini et al., 2016).

5. Conclusions

The present study is a further step in our attempts to couple AhR-reporter gene bioassay with proteomics in the risk assessment of SL and HC for humans and the environment. We can deduce the presence of other compounds besides organohalogens in SL and HC extracts from the biological effects observed. For example, the proteins found to be modulated suggest the action of heavy metals, identified as As and Cu by bioinformatic analysis and enriched in HC extract as reported by chemical analysis. Proteins modulated by HC and SL extracts were associated with antioxidant pathways, unfolded protein response and DNA damage that have close correlations with the effects of dioxin on the biological systems.

Moreover, the differential proteins identified here also play trigger roles in the onset of cancer and neurological disorders, as previously demonstrated in the zebrafish embryotoxicity test. In conclusion, the proteomic data highlights a scenario reconstructed by a holistic approach, which when combined with bioanalytical tools based on cell lines, proved useful for investigating the safety of complex matrices containing mixtures of chemicals toxic for humans and the environment.

Supplementary data to this article can be found online at https://doi.org/10.1016/j.scitotenv.2023.164651.

List of abbreviations

ACN	acetonitrile
BEQs	Bioanalytical Toxicity Equivalents
DSigDB	Drug SIGnatures DataBase
DR-CALUX	Dioxin responsive Chemically-activated-luciferase-gene-expression
CHAPS	(3-((3-cholamidopropyl) dimethylammonio)-1-propanesulfonate)
CTRL	un-treated H4IIE cells
DTE	ditioeritritolo

dl-PCBs	*dioxin-like* polychlorinated biphenyls
EPA	Environmental Protection Agency
GC–MS/MS	gas chromatograph tandem mass spectrometry
GO	Gene Ontology
HC	hydrochar
H4IIE	Cell line of Rat hepatoma
ICP-MS iCAP Q	Inductively Coupled Plasma-Mass Spectrometry with iCAP Q ™ technology
LOQ	limit of quantification
LOD	limit of detection
MALDI-ToF	Matrix assisted Laser Desorption Ionization Time of flight
MS	Mass Spectrometry
NRF2	Nuclear factor-erythroid 2-related factor 2
PBS	phosphate buffer saline
PCA	Principal Component Analysis
PC	principal component
PCDD/Fs	polychloro dibenzo-p-dioxins/furans
PCDFs	polychloro dibenzo-p-furans
PGC1	PPAR-γ co-activator-1 α
SL	Sewage sludge
SDS	Sodium Dodecyl Sulphate
SDS-PAGE	sodium dodecyl sulfate-polyacrylamide gel electrophoresis
TEQ	toxic equivalents
TFA	trifluoroacetic acid
TCDD	2,3,7,8-tetrachlorodibenzo-*p*-dioxin
2DE	two-dimensional electrophoresis
%V	percentage of relative volume

CRediT authorship contribution statement

Claudia Landi: Data curation, Formal analysis, Investigation, writing – original draft, Writing – review & editing. **Giulia Liberatori**: Data curation, Formal analysis, Investigation. **Monica Puccini**: Investigation, method, Writing – review & editing. **Enxhi Shaba**: Formal analysis, method. **Lorenza Vantaggiato**: Formal analysis, method. **Sandra Vitolo**: Writing – review & editing. **Ilaria Corsi**: Conceptualization, Supervision, Resources, Funding acquisition, writing – original draft, Writing – review & editing. **Luca Bini**: Supervision, Resources, Writing – review & editing.

Data availability

Data will be made available on request.

Declaration of competing interest

The authors declare the following financial interests/personal relationships which may be considered as potential competing interests: Ilaria Corsi reports financial support was provided by Tuscany Region.

Acknowledgements

References

Addeck, A., Croes, K., Van Langenhove, K., Denison, M.S., Elhamalawy, A., Elskens, M., Baeyens, W., 2014. Time-integrated monitoring of polychlorinated dibenzo-p-dioxins and polychlorinated dibenzofurans (PCDD/Fs) in urban and industrial wastewaters using a ceramic toximeter and the CALUX bioassay. Chemosphere 94, 27–35. https://doi.org/10.1016/j.chemosphere.2013.08.075.

Anderson, C.G., Joshi, G., Bair, D.A., Oriol, C., He, G., Parikh, S.J., Denison, M.S., Scow, K.M., 2017. Use of nuclear receptor luciferase-based bioassays to detect endocrine active chemicals in a biosolids-biochar amended soil. Chemosphere 181, 160–167. https://doi.org/10.1016/j.chemosphere.2017.04.035.

Azzaz, A.A., Khiari, B., Jellali, S., Ghimbeu, C.M., Jeguirim, M., 2020. Hydrochars production, characterization and application for wastewater treatment: a review. Renew. Sust. Energ. Rev. 127, 109882. https://doi.org/10.1016/j.rser.2020.109882.

Balu, N., Padgett, W.T., Lambert, G.R., Swank, A.E., Richard, A.M., Nesnow, S., 2004. Identification and characterization of novel stable deoxyguanosine and deoxyadenosine adducts of benzo[a]pyrene-7,8-quinone from reactions at physiological pH. Chem. Res. Toxicol. 17, 827–838. https://doi.org/10.1021/tx034207s.

Barceló, D., Žonja, B., Ginebreda, A., 2020. Toxicity tests in wastewater and drinking water treatment processes: a complementary assessment tool to be on your radar. J. Environ. Chem. Eng. 8, 104262. https://doi.org/10.1016/j.jece.2020.104262.

Bardhan, M., Novera, T.M., Tabassum, M., Islam, Md., Azharul, Islam, Atikul, Md., Hameed, B.H., 2021. Co-hydrothermal carbonization of different feedstocks to hydrochar as potential energy for the future world: a review. J. Clean. Prod. 298, 126734. https://doi.org/10.1016/j.jclepro.2021.126734.

Behnisch, P.A., Brouwer, B., 2020. Dioxins in food and feed – a never-ending story and lessons learned. Affidia - J. Food Diagn. 1, 44–49.

Behnisch, P.A., Hosoe, K., Sakai, S., 2001. Bioanalytical screening methods for dioxins and *dioxin-like* compounds—a review of bioassay/biomarker technology. Environ. Int. 27 (5), 413–439. https://doi.org/10.1016/s0160-4120(01)00028-9.

Behnisch, P.A., Umlauf, G., Stachel, B., Felzel, E., Brouwer, B., 2010. Bio/chemical analysis of sediment from Elbe River, the North Sea and from several tributaries. Organohalogen Compd. 72, 645–647.

Beníšek, M., Kukučka, P., Mariani, G., Suurkuusk, G., Gawlik, B.M., Locoro, G., Giesy, J.P., Bláha, L., 2015. Dioxins and dioxin-like compounds in composts and digestates from European countries as determined by the in vitro bioassay and chemical analysis. Chemosphere 122, 168–175. https://doi.org/10.1016/j.chemosphere.2014.11.039.

Besselink, H., Schipper, C., Klamer, H., Leonards, P., Verhaar, H., Felzel, E., Murk, A.J., Thain, J., Hosoe, K., Schoeters, G., Legler, J., Brouwer, B., 2004. Intra and Interlaboratory calibration of the DR CALUX® bioassay for the analysis of dioxins and *dioxin-like* chemicals in sediments. Environ. Toxicol. Chem. 23 (12), 2781–2789. https://doi.org/10.1897/03-542.1.

Cairns, R.A., Harris, I.S., Mak, T.W., 2011. Regulation of cancer cell metabolism. Nat. Rev. Cancer 11, 85–95. https://doi.org/10.1038/nrc2981.

Clarke, B.O., Smith, S.R., 2011. Review of "emerging" organic contaminants in biosolids and assessment of international research priorities for the agricultural use of biosolids. Environ. Int. 37, 226–247. https://doi.org/10.1016/j.envint.2010.06.004.

Das, D.N., Panda, P.K., Sinha, N., Mukhopadhyay, S., Naik, P.P., Bhutia, S.K., 2017. DNA damage by 2,3,7,8-tetrachlorodibenzo-p-dioxin-induced p53-mediated apoptosis through activation of cytochrome P450/aryl hydrocarbon receptor. Environ. Toxicol. Pharmacol. 55, 175–185. https://doi.org/10.1016/j.etap.2017.08.012.

Della Torre, C., Liberatori, G., Ghilardi, A., Del Giacco, L., Puccini, M., Ferraro, F., Vitolo, S., Corsi, I., 2022. The zebrafish (Danio rerio) embryo-larval contact assay combined with biochemical biomarkers and swimming performance in sewage sludge and hydrochar hazard assessment. Environ. Pollut. 302, 119053. https://doi.org/10.1016/j.envpol.2022.119053.

Eljarrat, E., Barceló, D., 2004. Sample handling and analysis of brominated flame retardants in soil and sludge samples. TrAC Trends Anal. Chem. 23, 727–736. https://doi.org/10.1016/j.trac.2004.07.009.

Escher, B.I., Stapleton, H.M., Schymanski, E.L., 2020. Tracking complex mixtures of chemicals in our changing environment. Science 367, 388–392. https://doi.org/10.1126/science.aay6636.

Farré, M., Barceló, D., 2003. Toxicity testing of wastewater and sewage sludge by biosensors, bioassays and chemical analysis. TrAC Trends Anal. Chem. 22, 299–310. https://doi.org/10.1016/S0165-9936(03)00504-1.

Fernandez, P.C., Frank, S.R., Wang, L., Schroeder, M., Liu, S., Greene, J., Cocito, A., Amati, B., 2003. Genomic targets of the human c-Myc protein. Genes Dev. 17, 1115–1129. https://doi.org/10.1101/gad.1067003.

Furue, M., Ishii, Y., Tsukimori, K., Tsuji, G., 2021. Aryl hydrocarbon receptor and dioxin-related health hazards-lessons from Yusho. Int. J. Mol. Sci. 22, E708. https://doi.org/10.3390/ijms22020708.

Fuse, Y., Nguyen, V.T., Kobayashi, M., 2016. Nrf2-dependent protection against acute sodium arsenite toxicity in zebrafish. Toxicol. Appl. Pharmacol. 305, 136–142. https://doi.org/10.1016/j.taap.2016.06.012.

Gianico, A., Braguglia, C.M., Gallipoli, A., Montecchio, D., Mininni, G., 2021. Land application of biosolids in Europe: possibilities, con-straints and future perspectives. Water 13, 103. https://doi.org/10.3390/w13010103.

Gievers, F., Loewen, A., Nelles, M., 2019. Hydrothermal carbonization (HTC) of sewage sludge: GHG emissions of various Hydrochar applications. In: Schebek, L., Herrmann, C., Cerdas, F. (Eds.), Progress in Life Cycle Assessment, Sustainable Production, Life Cycle Engineering and Management. Springer International Publishing, Cham, pp. 59–68 https://doi.org/10.1007/978-3-319-92237-9_7.

Graves, J.A., Metukuri, M., Scott, D., Rothermund, K., Prochownik, E.V., 2009. Regulation of reactive oxygen species homeostasis by peroxiredoxins and c-Myc. J. Biol. Chem. 284, 6520–6529. https://doi.org/10.1074/jbc.M807564200.

Gustavsson, L.K., Klee, N., Olsman, H., Hollert, H., Engwall, M., 2004. Fate of ah receptor agonists during biological treatment of an industrial sludge containing explosives and pharmaceutical residues. Environ. Sci. Pollut. Res. 11, 379–387. https://doi.org/10.1007/BF02979656.

Gustavsson, L., Hollert, H., Jönsson, S., van Bavel, B., Engwall, M., 2007. Reed beds receiving industrial sludge containing nitroaromatic compounds. Environ. Sci. Pollut. Res. Int. 14, 202–211. https://doi.org/10.1065/espr2006.11.360.

Hansen, J.M., Moriarty-Craige, S., Jones, D.P., 2007. Nuclear and cytoplasmic peroxiredoxin-1 differentially regulate NF-kappaB activities. Free Radic. Biol. Med. 43, 282–288. https://doi.org/10.1016/j.freeradbiomed.2007.04.029.

Heys, K.A., Shore, R.F., Pereira, M.G., Jones, K.C., Martin, F.L., 2016. Risk assessment of environmental mixture effects. RSC Adv. 6, 47844–47857. https://doi.org/10.1039/C6RA05406D.

Hoogenboom, R.L.A.P., ten Dam, G., van Bruggen, M., Jeurissen, S.M.F., van Leeuwen, S.P.J., Theelen, R.M.C., Zeilmaker, M.J., 2016. Polychlorinated dibenzo-p-dioxins and dibenzofurans (PCDD/Fs) and biphenyls (PCBs) in home-produced eggs. Chemosphere 150, 311–319. https://doi.org/10.1016/j.chemosphere.2016.02.034.

Hotamisligil, G.S., Davis, R.J., 2016. Cell signaling and stress responses. Cold Spring Harb. Perspect. Biol. 8, a006072. https://doi.org/10.1101/cshperspect.a006072.

Houtman, C.J., ten Broek, R., van Oorschot, Y., Kloes, D., van der Oost, R., Rosielle, M., Lamoree, M.H., 2020. High resolution effect-directed analysis of steroid hormone (ant) agonists in surface and wastewater quality monitoring. Environ. Toxicol. Pharmacol. 80, 103460. https://doi.org/10.1016/j.etap.2020.103460.

Huang, R., Tang, Y., 2015. Speciation dynamics of phosphorus during (hydro)thermal treatments of sewage sludge. Environ. Sci. Technol. 49, 14466–14474. https://doi.org/10.1021/acs.est.5b04140.

Iino, K., Toriumi, K., Agarie, R., Miyashita, M., Suzuki, K., Horiuchi, Y., Niizato, K., Oshima, K., Imai, A., Nagase, Y., Kushima, I., Koike, S., Ikegame, T., Jinde, S., Nagata, E., Washizuka, S., Miyata, T., Takizawa, S., Hashimoto, R., Kasai, K., Ozaki, N., Itokawa, M., Arai, M., 2021. AKR1A1 variant associated with schizophrenia causes exon skipping, leading to loss of enzymatic activity. Front. Genet. 12, 762999. https://doi.org/10.3389/fgene.2021.762999.

Jang, H.H., Lee, K.O., Chi, Y.H., Jung, B.G., Park, S.K., Park, J.H., Lee, J.R., Lee, S.S., Moon, J.C., Yun, J.W., Choi, Y.O., Kim, W.Y., Kang, J.S., Cheong, G.-W., Yun, D.-J., Rhee, S.G., Cho, M.J., Lee, S.Y., 2004. Two enzymes in one; two yeast peroxiredoxins display oxidative stress-dependent switching from a peroxidase to a molecular chaperone function. Cell 117, 625–635. https://doi.org/10.1016/j.cell.2004.05.002.

Kapanen, A., Vikman, M., Rajasärkkä, J., Virta, M., Itävaara, M., 2013. Biotests for environmental quality assessment of composted sewage sludge. Waste Manag. 33, 1451–1460. https://doi.org/10.1016/j.wasman.2013.02.022.

Kielkopf, C.L., Bauer, W., Urbatsch, I.L., 2020. Bradford assay for determining protein concentration. Cold Spring Harb Protoc 2020, 102269. https://doi.org/10.1101/pdb.prot102269.

Kortenkamp, A., Faust, M., 2018. Regulate to reduce chemical mixture risk. Science 361, 224–226. https://doi.org/10.1126/science.aat9219.

Kuleshov, M.V., Jones, M.R., Rouillard, A.D., Fernandez, N.F., Duan, Q., Wang, Z., Koplev, S., Jenkins, S.L., Jagodnik, K.M., Lachmann, A., McDermott, M.G., Monteiro, C.D., Gundersen, G.W., Ma'ayan, A., 2016. Enrichr: a comprehensive gene set enrichment analysis web server 2016 update. Nucleic Acids Res. 44, W90–W97. https://doi.org/10.1093/nar/gkw377.

Kumari, M., Kumar, A., 2020. Identification of component-based approach for prediction of joint chemical mixture toxicity risk assessment with respect to human health: a critical review. Food Chem. Toxicol. 143, 111458. https://doi.org/10.1016/j.fct.2020.111458.

Landi, C., Bargagli, E., Carleo, A., Bianchi, L., Gagliardi, A., Prasse, A., Perari, M.G., Refini, R.M., Bini, L., Rottoli, P., 2014. A system biology study of BALF from patients affected by idiopathic pulmonary fibrosis (IPF) and healthy controls. Proteomics Clin. Appl. 8, 932–950. https://doi.org/10.1002/prca.201400001.

Landi, C., Liberatori, G., Cotugno, P., Sturba, L., Vannuccini, M.L., Massari, F., Miniero, D.V., Tursi, A., Shaba, E., Behnisch, P.A., Carleo, A., Di Giuseppe, F., Angelucci, S., Bini, L., Corsi, I., 2021. First attempt to couple proteomics with the AhR reporter gene bioassay in soil pollution monitoring and assessment. Toxics 10, 9. https://doi.org/10.3390/toxics10010009.

Lanzafame, M., Branca, G., Landi, C., Qiang, M., Vaz, B., Nardo, T., Ferri, D., Mura, M., Iben, S., Stefanini, M., Peverali, F.A., Bini, L., Orioli, D., 2021. Cockayne syndrome group A and ferrochelatase finely tune ribosomal gene transcription and its response to UV irradiation. Nucleic Acids Res. 49, 10911–10930. https://doi.org/10.1093/nar/gkab819.

Liberatori, G., Mazzoli, C., Ferraro, F., Sturba, L., Vannuccini, M.L., Baroni, D., Behnisch, P.A., Puccini, M., Vitolo, S., Corsi, I., 2022. Aryl hydrocarbon reporter gene bioassay for screening polyhalogenated dibenzo-p-dioxins/furans and dioxin-like polychlorinated biphenyls in hydrochar and sewage sludge. J. Hazard. Mater. 428, 128256. https://doi.org/10.1016/j.jhazmat.2022.128256.

Liu, G.Y., Sabatini, D.M., 2020. mTOR at the nexus of nutrition, growth, ageing and disease. Nat. Rev. Mol. Cell Biol. 21, 183–203. https://doi.org/10.1038/s41580-019-0199-y.

Liu, X., Li, Z., Liu, S., Sun, J., Chen, Z., Jiang, M., Zhang, Q., Wei, Y., Wang, X., Huang, Y.-Y., Shi, Y., Xu, Y., Xian, H., Bai, F., Ou, C., Xiong, B., Lew, A.M., Cui, J., Fang, R., Huang, H., Zhao, J., Hong, X., Zhang, Y., Zhou, F., Luo, H.-B., 2020. Potential therapeutic effects of dipyridamole in the severely ill patients with COVID-19. Acta Pharm. Sin. B 10, 1205–1215. https://doi.org/10.1016/j.apsb.2020.04.008.

Lyu, H., He, Y., Tang, J., Hecker, M., Liu, Q., Jones, P.D., Codling, G., Giesy, J.P., 2016. Effect of pyrolysis temperature on potential toxicity of biochar if applied to the environment. Environ. Pollut. 218, 1–7. https://doi.org/10.1016/j.envpol.2016.08.014.

Macova, M., Toze, S., Hodgers, L., Mueller, J.F., Bartkow, M., Escher, B.I., 2011. Bioanalytical tools for the evaluation of organic micropollutants during sewage treatment, water recycling and drinking water generation. Water Res. 45, 4238–4247. https://doi.org/10.1016/j.watres.2011.05.032.

Maniscalco, M.P., Volpe, M., Messineo, A., 2020. Hydrothermal carbonization as a valuable tool for energy and environmental applications: a review. Energies 13, 4098. https://doi.org/10.3390/en13164098.

Maréchal, A., Zou, L., 2013. DNA damage sensing by the ATM and ATR kinases. Cold Spring Harb. Perspect. Biol. 5, a012716. https://doi.org/10.1101/cshperspect.a012716.

Masoumi, S., Borugadda, V.B., Nanda, S., Dalai, A.K., 2021. Hydrochar: a review on its production technologies and applications. Catalysts 11, 939. https://doi.org/10.3390/catal11080939.

Mattaini, K.R., Sullivan, M.R., Vander Heiden, M.G., 2016. The importance of serine metabolism in cancer. J. Cell Biol. 214, 249–257. https://doi.org/10.1083/jcb.201604085.

Milieu Ltd, WRc, Risk and Policy Analysts Ltd (RPA), 2010. Environmental, economic and social impacts of the use of sewage sludge on land. Final Report, Part III: Project Interim Reports DG ENV.G.4./ETU/2008/0076r, Brussels, Belgium http://ec.europa.eu/environment/archives/waste/sludge/pdf/part_iii_report.pdf.

Neale, P.A., Braun, G., Brack, W., Carmona, E., Gunold, R., König, M., Krauss, M., Liebmann, L., Liess, M., Link, M., Schäfer, R.B., Schlichting, R., Schreiner, V.C., Schulze, T., Vormeier, P., Weisner, O., Escher, B.I., 2020. Assessing the mixture effects in in vitro bioassays of chemicals occurring in small agricultural streams during rain events. Environ. Sci. Technol. https://doi.org/10.1021/acs.est.0c02235.

Oakley, B.R., Kirsch, D.R., Morris, N.R., 1980. A simplified ultrasensitive silver stain for detecting proteins in polyacrylamide gels. Anal. Biochem. 105, 361–363. https://doi.org/10.1016/0003-2697(80)90470-4.

Ontañon, O.M., Landi, C., Carleo, A., Gagliardi, A., Bianchi, L., González, P.S., Agostini, E., Bini, L., 2018. What makes a. guillouiae SFC 500-1A able to co-metabolize phenol and Cr(VI)? A proteomic approach. J. Hazard. Mater. 354, 215–224. https://doi.org/10.1016/j.jhazmat.2018.04.068.

Panjali, Z., Hahad, O., Rajabi, F., Maddah, S., Zendehdel, R., 2021. Occupational exposure to metal-rich particulate matter modifies the expression of repair genes in foundry workers. Toxicol. Ind. Health 37, 504–512. https://doi.org/10.1177/07482337211021202.

Perez-Riverol, Y., Csordas, A., Bai, J., Bernal-Llinares, M., Hewapathirana, S., Kundu, D.J., Inuganti, A., Griss, J., Mayer, G., Eisenacher, M., Pérez, E., Uszkoreit, J., Pfeuffer, J., Sachsenberg, T., Yilmaz, S., Tiwary, S., Cox, J., Audain, E., Walzer, M., Jarnuczak, A.F., Ternent, T., Brazma, A., Vizcaíno, J.A., 2019. The PRIDE database and related tools and resources in 2019: improving support for quantification data. Nucleic Acids Res. 47, D442–D450. https://doi.org/10.1093/nar/gky1106.

Protano, G., Baroni, F., Di Lella, L.A., Mazzoni, A., Nannoni, F., Papale, A., 2020. How do properties and heavy metal levels change in soils fertilized with regulated doses of urban sewage sludge in the framework of a real agronomic treatment program? J. Soils Sediments 20, 1383–1394. https://doi.org/10.1007/s11368-019-02511-3.

Rhind, N., Russell, P., 2012. Signaling pathways that regulate cell division. Cold Spring Harb. Perspect. Biol. 4, a005942. https://doi.org/10.1101/cshperspect.a005942.

Rorat, A., Courtois, P., Vandenbulcke, F., Lemiere, S., 2019. 8 - sanitary and environmental aspects of sewage sludge management. In: Prasad, M.N.V., de Campos Favas, P.J., Vithanage, M., Mohan, S.V. (Eds.), Industrial and Municipal Sludge. Butterworth-Heinemann, pp. 155–180 https://doi.org/10.1016/B978-0-12-815907-1.00008-8.

Rosenfeldt, M.T., Ryan, K.M., 2009. The role of autophagy in tumour development and cancer therapy. Expert Rev. Mol. Med. 11, e36. https://doi.org/10.1017/S1462399409001306.

Schaub, F.X., Dhankani, V., Berger, A.C., Trivedi, M., Richardson, A.B., Shaw, R., Zhao, W., Zhang, X., Ventura, A., Liu, Y., Ayer, D.E., Hurlin, P.J., Cherniack, A.D., Eisenman, R.N., Bernard, B., Grandori, C., Cancer Genome Atlas Network, 2018. Pan-cancer alterations of the MYC oncogene and its proximal network across the cancer genome atlas. Cell Syst. 6, 282–300.e2. https://doi.org/10.1016/j.cels.2018.03.003.

Selivanovskaya, S.Yu., Latypova, V.Z., 2003. The use of bioassays for evaluating the toxicity of sewage sludge and sewage sludge-amended soil. J. Soils Sediments 3, 85–92. https://doi.org/10.1007/BF02991073.

Singh, R., Sharma, R., Tewari, N., Geetanjali, Rawat, D.S., 2006. Nitrilase and its application as a "green" catalyst. Chem. Biodivers. 3, 1279–1287. https://doi.org/10.1002/cbdv.200690131.

Sinha, P., Poland, J., Schnölzer, M., Rabilloud, T., 2001. A new silver staining apparatus and procedure for matrix-assisted laser desorption/ionization-time of flight analysis of proteins after two-dimensional electrophoresis. Proteomics 1, 835–840. https://doi.org/10.1002/1615-9861(200107)1:7<835::AID-PROT835>3.0.CO;2-2.

Suzuki, G., Takigami, H., Kushi, Y., Sakai, S., 2004. Evaluation of mixture effects in a crude extract of compost using the CALUX bioassay and HPLC fractionation. Environ. Int. 30, 1055–1066. https://doi.org/10.1016/j.envint.2004.05.005.

Takigami, H., Suzuki, G., Sakai, S., 2010. Screening of dioxin-like compounds in bio-composts and their materials: chemical analysis and fractionation-directed evaluation of AhR ligand activities using an in vitro bioassay. J. Environ. Monit. 12, 2080–2087. https://doi.org/10.1039/C0EM00200C.

Tasca, A.L., Stefanelli, E., Raspolli Galletti, A.M., Gori, R., Mannarino, G., Vitolo, S., Puccini, M., 2020. Hydrothermal carbonization of sewage sludge: analysis of process severity and solid content. Chem. Eng. Technol. 43, 2382–2392. https://doi.org/10.1002/ceat.202000095.

Tomczyk, B., Siatecka, A., Bogusz, A., Oleszczuk, P., 2021. Ecotoxicological assessment of sewage sludge-derived biochars-amended soil. Environ. Pollut. 275, 116484. https://doi.org/10.1016/j.envpol.2021.116484.

Tong, X.-J., Li, Q.-J., Duan, Y.-M., Liu, N.-N., Zhang, M.-L., Zhou, J.-Q., 2011. Est1 protects telomeres and inhibits subtelomeric y'-element recombination. Mol. Cell. Biol. 31, 1263–1274. https://doi.org/10.1128/MCB.00831-10.

Van den Berg, M., Birnbaum, L.S., Denison, M., De Vito, M., Farland, W., Feeley, M., Fiedler, H., Hakansson, H., Hanberg, A., Haws, L., Rose, M., Safe, S., Schrenk, D., Tohyama, C., Tritscher, A., Tuomisto, J., Tysklind, M., Walker, N., Peterson, R.E., 2006. The 2005 World Health Organization reevaluation of human and mammalian toxic equivalency factors for dioxins and dioxin-like compounds. Toxicol. Sci. 93, 223–241. https://doi.org/10.1093/toxsci/kfl055.

Van Langenhove, K., Dumortier, P., Scholl, G., Denison, M.S., Pussemier, L., Focant, J.F., Goeyens, L., Baeyens, W., Elskens, M., 2012. Analysis of PCDD/fs and dioxin-like PCBs in sewage sludges and general bio-wastes available for agricultural land application in Belgium - comparison between GC-IDHRMS and CALUX results. Organohalogen Compd. 74, 206–209.

Wang, X., He, S., Sun, J.-M., Delcuve, G.P., Davie, J.R., 2010. Selective association of peroxiredoxin 1 with genomic DNA and COX-2 upstream promoter elements in estrogen receptor negative breast cancer cells. Mol. Biol. Cell 21, 2987–2995. https://doi.org/10.1091/mbc.E10-02-0160.

Wang, Y.A., Sun, Y., Le Blanc, J.M., Solomides, C., Zhan, T., Lu, B., 2016. Nitrilase 1 modulates lung tumor progression in vitro and in vivo. Oncotarget 7, 21381–21392. https://doi.org/10.18632/oncotarget.7820.

Wiedner, K., Naisse, C., Rumpel, C., Pozzi, A., Wieczorek, P., Glaser, B., 2013. Chemical modification of biomass residues during hydrothermal carbonization – what makes the difference, temperature or feedstock? Org. Geochem. 54, 91–100. https://doi.org/10.1016/j.orggeochem.2012.10.006.

Yuan, Q., Sallach, J.B., Rhodes, G., Bach, A., Crawford, R., Li, H., Johnston, C.T., Teppen, B.J., Kaminski, N.E., Boyd, S.A., 2021. Natural organic matter does not diminish the mammalian bioavailability of 2,3,7,8-tetrachlorodibenzo-p-dioxin. Chemosphere 264, 128420. https://doi.org/10.1016/j.chemosphere.2020.128420.

Zhang, T., Yu, G., Wang, B., Fiedler, H., Huang, J., Deng, S., 2009. Bioanalytical characterization of dioxin-like activity in sewage sludge from Beijing, China. Chemosphere 75, 649–653. https://doi.org/10.1016/j.chemosphere.2008.12.064.